Energy Minimization Based Segmentation and Denoising Using a Multilayer Level Set Approach*

Ginmo Chung and Luminita A. Vese

Department of Mathematics, University of California, Los Angeles,
405 Hilgard Avenue, Los Angeles, CA 90095-1555, USA
senninha@math.ucla.edu, lvese@math.ucla.edu

Abstract. This paper is devoted to piecewise-constant segmentation of images using a curve evolution approach in a variational formulation. The problem to be solved is also called the minimal partition problem, as formulated by Mumford and Shah [20]. The proposed new models are extensions of the techniques previously introduced in [9], [10], [27]. We represent here the set of boundaries of the segmentation implicitly, by a multilayer of level-lines of a continuous function. In the standard approach of front propagation, only one level line is used to represent the boundary. The multilayer idea is inspired from previous work on island dynamics for epitaxial growth [14], [4]. Using a multilayer level set approach, the computational cost is smaller and in some applications, a nested structure of the level lines can be useful.

1 Introduction

We model here images by functions $f : \Omega \to I\!R$, where Ω is an open and bounded domain in $I\!R^n$. In particular, $n = 1$ corresponds to signals, $n = 2$ corresponds to planar images, while $n = 3$ corresponds to volumetric images, such as MRI data.

An important problem in image analysis is the segmentation or the partition of an image f into regions and their boundaries, such that the regions correspond to objects in the scene. Here, we deal with the case where we look for an optimal piecewise-constant approximation of the function f, our starting point being the minimal partition problem, as formulated by D. Mumford and J. Shah [20]. The general problem is, given a function f in $L^\infty(\Omega)$ (induced by the L^2-topology), find a set of disjoint open regions Ω_i, such that $u = c_i$ in each Ω_i is a minimizer of [20]

$$F(u, \Gamma) = \sum_i \int_{\Omega_i} |f - c_i|^2 dx + \mu \mathcal{H}^{n-1}(\Gamma), \tag{1}$$

* This work has been supported in part by the National Science Foundation (Grants NSF ITR ACI-0113439 and NSF DMS 0312222), by an Alfred P. Sloan Fellowship, by the National Institute of Mental Health and the National Institute of Neurological Disorders and Stroke (Grant MH65166), and by the Institute of Pure and Applied Mathematics.

A. Rangarajan et al. (Eds.): EMMCVPR 2005, LNCS 3757, pp. 439–455, 2005.

where $\Gamma = \cup_i(\partial\Omega_i)$, $\Omega = (\cup_i\Omega_i) \cup \Gamma$, $\mu > 0$ is a scale parameter, and $\mathcal{H}^{n-1}$ is the Hausdorff $(n-1)$-dimensional measure in $\mathbb{R}^n$. In one dimension $\mathcal{H}^0(\Gamma)$ is the counting measure, in two dimensions $\mathcal{H}^1(\Gamma)$ is the length of the curve Γ, while in three dimensions $\mathcal{H}^2(\Gamma)$ is the surface area.

The existence of minimizers has been proved by Mumford-Shah for continuous data f [20], and later by Morel-Solimini [19], for data $f \in L^\infty(\Omega)$. Elliptic convergent approximations of the minimal partition problem in the weak formulation (and also of the full Mumford and Shah model) have been proposed by Ambrosio-Tortorelli [1], [2], where the minimizer u is approximated by smoother functions, and the unknown set of discontinuities is also approximated by a smooth function v, essentially supported outside Γ. A constructive convergent algorithm for solving (1) has been proposed by Koepfler-Lopez-Morel [16], based on region growing and merging (a piecewise-constant minimizer u is obtained, and not only a smooth approximation, by contrast with [1], [2]). Also, it has been proved by Mumford-Shah [20] that a minimizer u of (1) has a finite number of regions Ω_i and of constant intensities c_i.

Curve evolution techniques and implicit representations for global segmentation have been proposed, that can be seen as particular cases of the minimal partition problem, where the number of regions Ω_i or an upper bound are assumed to be known. Thus, in [9], [10], [8], [27], [28], restrictions of the energy (1) to piecewise-constant functions taking a finite number of regions and intensities, in a variational level set approach [29], have been introduced. The energy has been minimized for restrictions to $\{u(x) = c_1H(\phi(x))+c_2H(-\phi(x))\}$, or $\{u(x) = c_{11}H(\phi_1(x))H(\phi_2(x)) + c_{10}H(\phi_1(x))H(-\phi_2(x)) + c_{01}H(-\phi_1(x))H(\phi_2(x)) + c_{00}H(-\phi_1(x))H(-\phi_2(x))\}$, and so on, where $\phi, \phi_i : \Omega \to \mathbb{R}$ are Lipschitz continuous functions, and H denotes the Heaviside function. The variational level set approach from Zhao, Chan, Merriman, and Osher [29] has been used, and the boundaries were represented by zero level lines of ϕ_i.

The multiphase formulation from [29] has been used in [24], [25] for computing the boundaries $\partial\Omega_i$ in the case of a finite and known number of regions, and where the corresponding intensity averages c_i where given.

The advantage of the multiphase method in [27] is that triple junctions can be represented, as in [29], [24], [25], but the regions Ω_i are disjoint and covering of Ω by definition. In addition, a smaller number of level set functions ϕ_i was needed to represent the partition, for the same number of distinct intensities c_i.

In the above mentioned work, together with other related work, the unknown boundaries $\partial\Omega_i$ are represented by the zero level line of a Lipschitz continuous function ϕ. In general, such function $\phi : \Omega \to \mathbb{R}$, as used for active contours [5], [18], [6], [15] partitions the domain Ω in at most two open regions $\{x \in \Omega : \phi(x) > 0\}$ and $\{x \in \Omega : \phi(x) < 0\}$, with a common boundary given by the zero level line of ϕ, $\{x \in \Omega : \phi(x) = 0\}$. For image partition, active contours, and image segmentation, such functions ϕ are thus used to represent boundaries of regions of different characteristics. In order to represent more than two regions, several functions ϕ_i can be combined and used, as we have mentioned in [29], [24], [25], [27]. For instance, in [11], [27], only two functions ϕ_i, $i = 1, 2$ were used

to represent up to four disjoint regions making up Ω, and only three functions ϕ_i, $i = 1, 2, 3$ were used to represent up to eight disjoint regions.

Here, we continue the approaches from [9], [10], [27], and we show that we can use even fewer level set functions to represent disjoint regions making up Ω. The applications illustrated in this paper include active contours for object detection, image segmentation and partition, image denoising. The main idea is to use more than one level-line of the Lipschitz continuous function ϕ to represent the discontinuity set of u, and the computational cost is decreased. The idea is inspired from a different application of implicit curve evolution and free boundaries, introduced in [14], [4], where island dynamics for epitaxial growth is modeled. A first layer of islands is represented by $\{x : \ \phi(x) = 0\}$, then a second layer of islands, growing on the top of the previous one is represented as $\{x : \ \phi(x) = 1\}$, etc.

In summary, here we combine the techniques from [9], [10], [27] for image partition, with the multilayer technique for modeling epitaxial growth from [14], [4], to obtain new and improved curve evolution models for image segmentation. Another recent independent work for image segmentation is Lie, Lysaker and Tai [17], where the authors propose an interesting and efficient multi-phase image segmentation model using a polynomial approach, but different than the methods proposed in the present work.

The proposed minimization methods are non-convex, and with no uniqueness for global minimizers (these theoretical properties are inherited from the Mumford and Shah model). Moreover, we do not guarantee that our multilayer formulation computes a global minimizer of the energy. It is possible sometime to obtain only a local minimizer by the computational algorithm. Also, the final result may depend on the choice of the initialization. However, in practice, we have obtained very satisfactory results; the numerical algorithm is stable and the computed energy is decreasing function of iterations, to a local or global minimizer. The method is computationally more efficient than the one introduced in [27]. Related prior work for region based segmentation using curve evolution implementation is by L. Cohen [12], [13], Paragios-Deriche [21], [22], [23], Tsai, Yezzi and Willsky [26], among other work mentioned in [27]. We also mention the segmentation model by Zhu-Yuille, in a probabilistic energy minimization approach [30].

2 Description of the Proposed Models

2.1 The Case of One Function

We consider in this subsection the case when the contours in the image f can be represented by level lines of the same level set function ϕ.

Two Levels. Let us consider a Lipschitz continuous function $\phi : \Omega \to I\!R$. Using for instance two levels $l_1 = 0$ and $l_2 = l > 0$, the function ϕ partitions the domain into three disjoint open regions, making up Ω, together with their boundaries:

$$R_1 = \{x:\ \phi(x) < 0\},\ R_2 = \{x:\ 0 < \phi(x) < l\},\ R_3 = \{x:\ \phi(x) > l\}.$$

We can thus extend the binary piecewise-constant level set segmentation model from [9], [10], to the following model, again as an energy minimization algorithm, in a level set form:

$$\inf_{c_1,c_2,c_3,\phi} F(c_1,c_2,c_3,\phi) = \int_\Omega |f(x)-c_1|^2 H(-\phi(x))dx \tag{2}$$
$$+ \int_\Omega |f(x)-c_2|^2 H(\phi(x))H(l-\phi(x))dx + \int_\Omega |f(x)-c_3|^2 H(\phi(x)-l)dx$$
$$+ \mu\Big[\int_\Omega |\nabla H(\phi)| + \int_\Omega |\nabla H(\phi-l)|\Big],$$

where H is the one-dimensional Heaviside function, and $\mu > 0$ is a weight parameter. The terms $\int_\Omega |\nabla H(\phi)|$ and $\int_\Omega |\nabla H(\phi - l)|$ correspond to the length of the boundary between R_1, R_2 and R_2, R_3, respectively. The segmented image in this case will be given by

$$u(x) = c_1 H(-\phi(x)) + c_2 H(\phi(x))H(l-\phi(x)) + c_3 H(\phi(x)-l).$$

To minimize the above energy, we approximate the Heaviside function by a regularized version H_ε, as $\varepsilon \to 0$, such that $H_\varepsilon \to H$ pointwise and $H_\varepsilon \in C^1(I\!R)$. We denote by $\delta_\varepsilon := H'_\varepsilon$. Examples of such approximations, that we use in practice, are [9], [10]:

$$H_\varepsilon(z) = \frac{1}{2}\Big(1 + \frac{2}{\pi} arctan(\frac{z}{\varepsilon})\Big), \quad \delta_\varepsilon(z) = H'_\varepsilon(z) = \frac{1}{\pi}\cdot\frac{\varepsilon}{\varepsilon^2+z^2}.$$

Minimizing the corresponding approximate energy F_ε alternately with respect to the unknowns, yields the associated Euler-Lagrange equations, parameterizing the descent direction by an artificial time $t \geq 0$:

$$\phi(0,x) = \phi_0(x), \tag{3}$$
$$c_1(t) = \frac{\int_\Omega f(x)H(-\phi(t,x))dx}{\int_\Omega H(-\phi(t,x))dx}, \tag{4}$$
$$c_2(t) = \frac{\int_\Omega f(x)H(\phi(t,x))H(l-\phi(t,x))dx}{\int_\Omega H(\phi(t,x))H(l-\phi(t,x))dx}, \tag{5}$$
$$c_3(t) = \frac{\int_\Omega f(x)H(\phi(t,x)-l)dx}{\int_\Omega H(\phi(t,x)-l)dx}, \tag{6}$$
$$\frac{\partial\phi}{\partial t} = \delta_\varepsilon(\phi)\Big[|f-c_1|^2 - |f-c_2|^2 H(l-\phi) + \mu \mathrm{div}\Big(\frac{\nabla\phi}{|\nabla\phi|}\Big)\Big] \tag{7}$$
$$+\delta_\varepsilon(\phi-l)\Big[H(\phi)|f-c_2|^2 - |f-c_3|^2 + \mu\mathrm{div}\Big(\frac{\nabla\phi}{|\nabla\phi|}\Big)\Big],$$
$$\frac{(\delta_\varepsilon(\phi)+\delta_\varepsilon(\phi-l))\nabla\phi}{|\nabla\phi|}\cdot\boldsymbol{n} = 0 \text{ on } \partial\Omega,\ t>0, \tag{8}$$

where $\boldsymbol{n}$ is the exterior unit normal to $\partial\Omega$. At steady state, a local or global minimizer of the energy (2) will be obtained. Note that the energy (2) is non-convex and it may have more than one global minimizer, these being properties inherited from the Mumford and Shah model [20]. In practice, we do not guarantee that our computational algorithm converges to a global minimizer. Therefore, sometime only a local minimizer may be obtained, but close to a global minimizer, and this may also depend on the choice of the initialization of the algorithm.

***m* Levels.** More levels $\{l_1 < l_2 < ... < l_m\}$ can be considered, instead of only two $\{l_1 = 0 < l_2 = l\}$. The energy in this more general case will be:

$$\begin{aligned}\inf_{c_1,c_2,...,c_{m+1},\phi} F(c_1,c_2,...,c_{m+1},\phi) &= \int_\Omega |f(x)-c_1|^2 H(l_1-\phi(x))dx \\ &+ \sum_{i=2}^{m}\int_\Omega |f(x)-c_i|^2 H(\phi(x)-l_{i-1})H(l_i-\phi(x))dx \\ &+ \int_\Omega |f(x)-c_{m+1}|^2 H(\phi(x)-l_m)dx + \mu\sum_{i=1}^{m}\int_\Omega |\nabla H(\phi-l_i)|.\end{aligned}$$

The associated Euler-Lagrange equations in this more general case, can be expressed in a similar way, as follows: in a dynamical scheme, starting with $\phi(0,x) = \phi_0(x)$, solve for $t > 0$

$$\begin{aligned}c_1(t) &= \frac{\int_\Omega f(x)H(l_1-\phi(t,x))dx}{\int_\Omega H(l_1-\phi(t,x))dx},\\ c_i(t) &= \frac{\int_\Omega f(x)H(\phi(t,x)-l_{i-1})H(l_i-\phi(t,x))dx}{\int_\Omega H(\phi(t,x)-l_{i-1})H(l_i-\phi(t,x))dx},\\ c_{m+1}(t) &= \frac{\int_\Omega f(x)H(\phi(t,x)-l_m)dx}{\int_\Omega H(\phi(t,x)-l_m)dx},\end{aligned}$$

for $i = 2, ..., m$, and

$$\begin{aligned}\frac{\partial\phi}{\partial t} &= \delta_\varepsilon(l_1-\phi)|f-c_1|^2 + \sum_{i=2}^{m}\Big[-\delta_\varepsilon(\phi-l_{i-1})H(l_i-\phi)|f-c_i|^2 \\ &+ \delta_\varepsilon(l_i-\phi)H(\phi-l_{i-1})|f-c_i|^2\Big] - \delta_\varepsilon(\phi-l_m)|f-c_{m+1}|^2 \\ &+ \mu\sum_{i=1}^{m}\Big[\delta_\varepsilon(\phi-l_i)\mathrm{div}\Big(\frac{\nabla\phi}{|\nabla\phi|}\Big)\Big],\end{aligned}$$

together with the corresponding boundary conditions on $\partial\Omega$, for $t > 0$.

We show in Fig. 1 examples of partitions of the domain Ω, using two and three level lines of a Lipschitz continuous function ϕ.

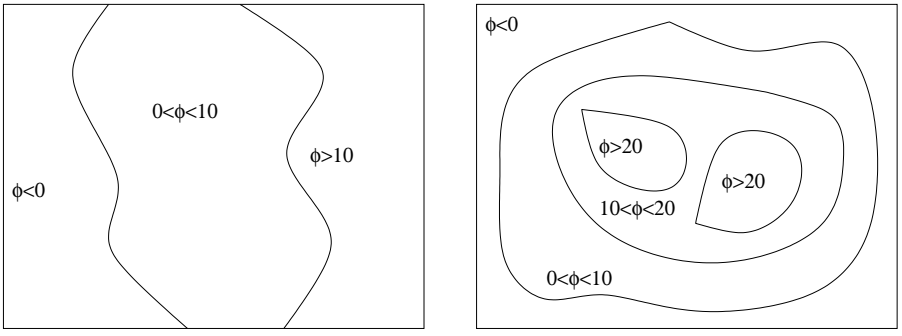

Fig. 1. Left: the level lines $\{x \in \Omega : \ \phi(x) = 0\}$, $\{x \in \Omega : \ \phi(x) = 10\}$ partition the domain Ω into 3 disjoint regions. Right: the level lines $\{x \in \Omega : \ \phi(x) = 0\}$, $\{x \in \Omega : \ \phi(x) = 10\}$, $\{x \in \Omega : \ \phi(x) = 20\}$ partition the domain Ω into 4 disjoint regions.

We present next experimental results applied to synthetic and real images obtained with the models with one level set function and multiple layers just introduced. In each figure, we show the evolution over time of the segmented image u of averages (left column), and the evolving set of curves superposed over the initial image f (right column). We also give the main parameters used in the calculations and the CPU times.

In Fig. 2 we illustrate how the model works on a noisy synthetic image, in the case $m = 3$, where m is the number of the nested level lines of the function ϕ used to partition the domain Ω. In Fig. 3-4, we illustrate how the models work on real noisy images of poor resolution, representing blood cells. Here, the model with two level lines of the function ϕ has been applied, producing very satisfactory results. In Fig. 5, application to brain data segmentation is illustrated.

We note that in all these cases, in the piecewise-constant segmentation models from [24], [25], and [27], we would have needed more than one function ϕ for the segmentation, therefore more computational storage is required. In practice, we do not impose that ϕ is Lipschitz continuous (this aspect will be discussed again at the end). The parameter levels l_1, l_2, ... are here kept constant and fixed for all our different experimental calculations. These can also be specified by the user. We have not implemented an automatic procedure of selection of these parameter levels. Sometimes, these could be estimated if a statistical prior exists about the contours or level lines of the data. We note that the algorithm is not sensitive with respect to the change of these parameter levels l_i. As in the model from [27], only an upper bound of the phases is needed. For instance we can segment an image into 2 regions, using the model with one level set function and 2 levels (therefore with 3 regions in theory, but only two regions will appear in practice). Note that in all cases, the energy reaches a minimum (local or global) very fast, only after a small number of iterations. The only varying parameter in this set of results is the coefficient of the length term, which has a scaling role.

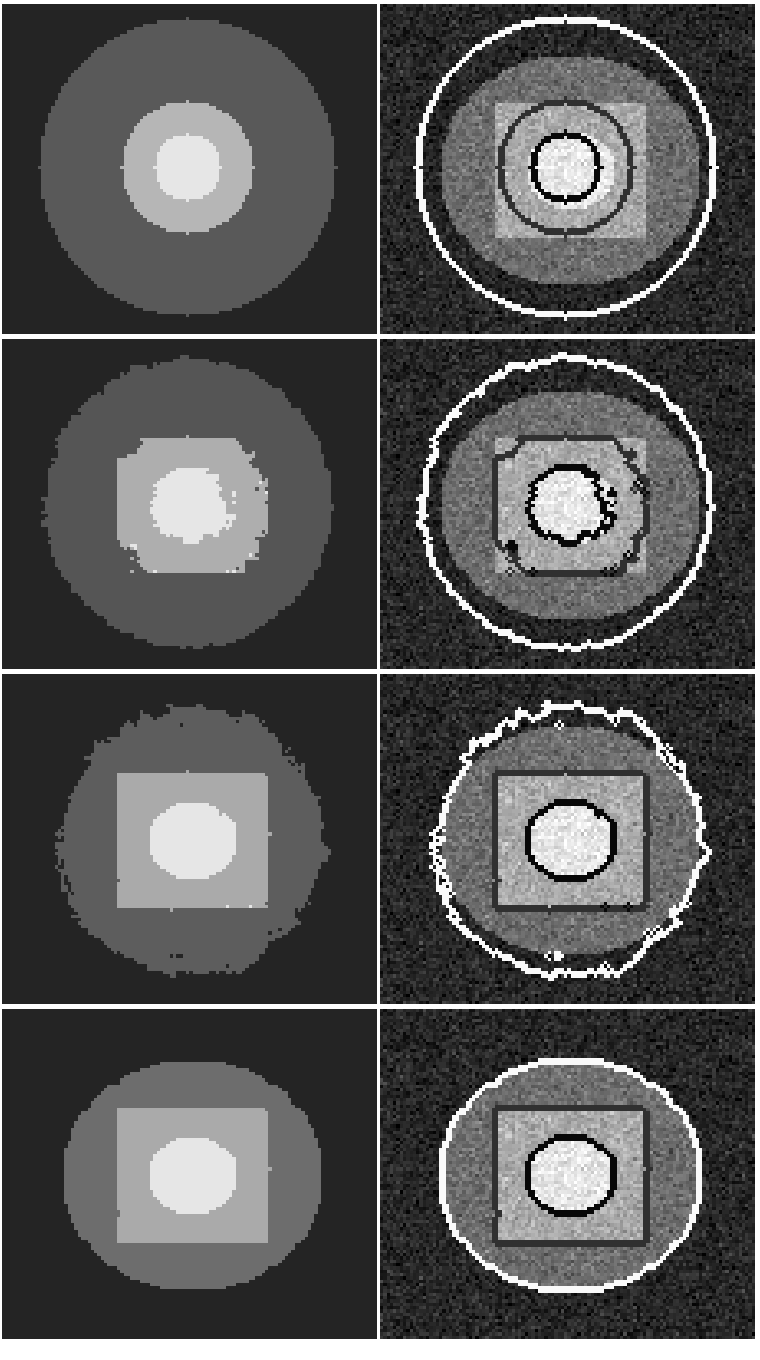

Fig. 2. Segmentation and denoising of a noisy synthetic image using one level set function ϕ and 3 levels. Parameters: $l_1 = 0, l_2 = 25, l_3 = 35, \triangle t = 0.1, \mu = 0.0217 \cdot 255^2$, 30 iterations, cpu time 0.41 sec.

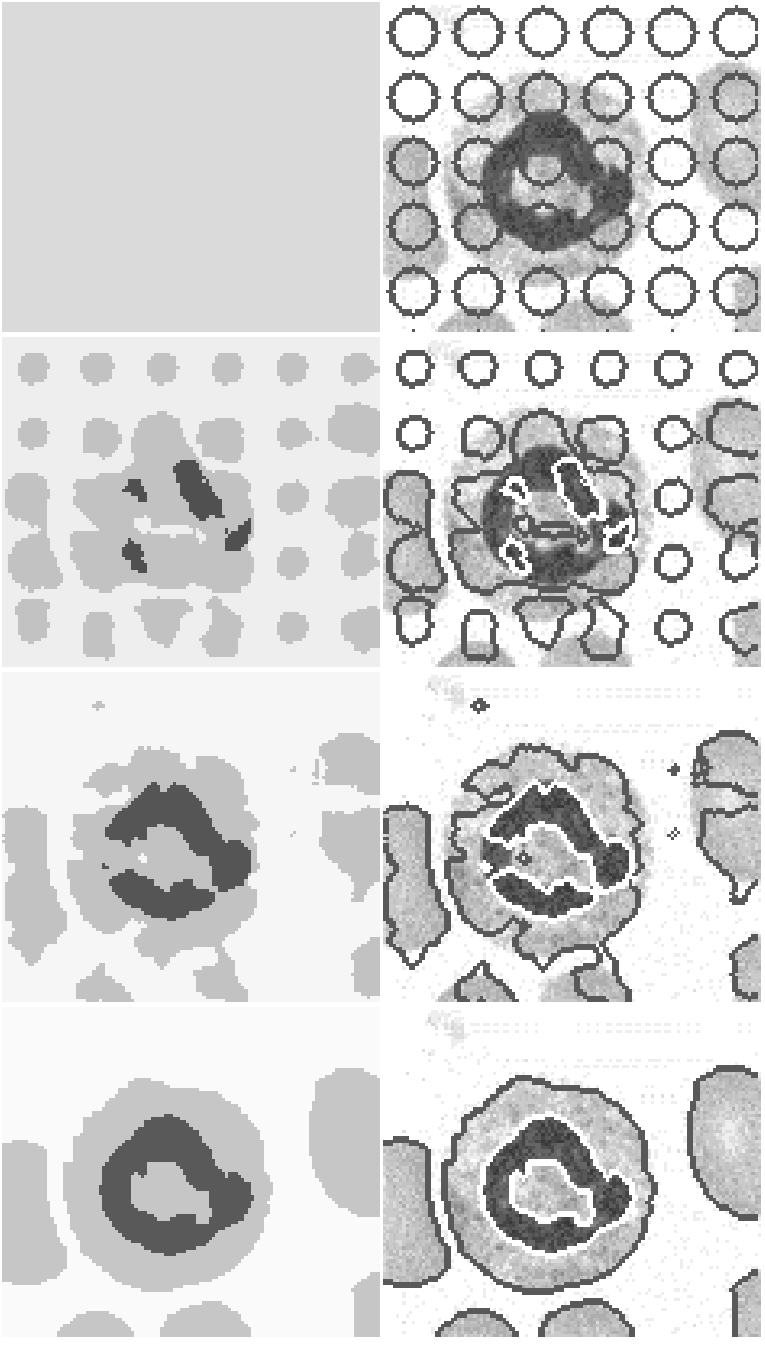

Fig. 3. Segmentation and denoising of a real noisy blood cells image using one level set function and two levels. Parameters: $l_1 = 0$, $l_2 = 25$, $\triangle t = 0.1$, $\mu = 0.03 \cdot 255^2$, 200 iterations, cpu time 2.51 sec.

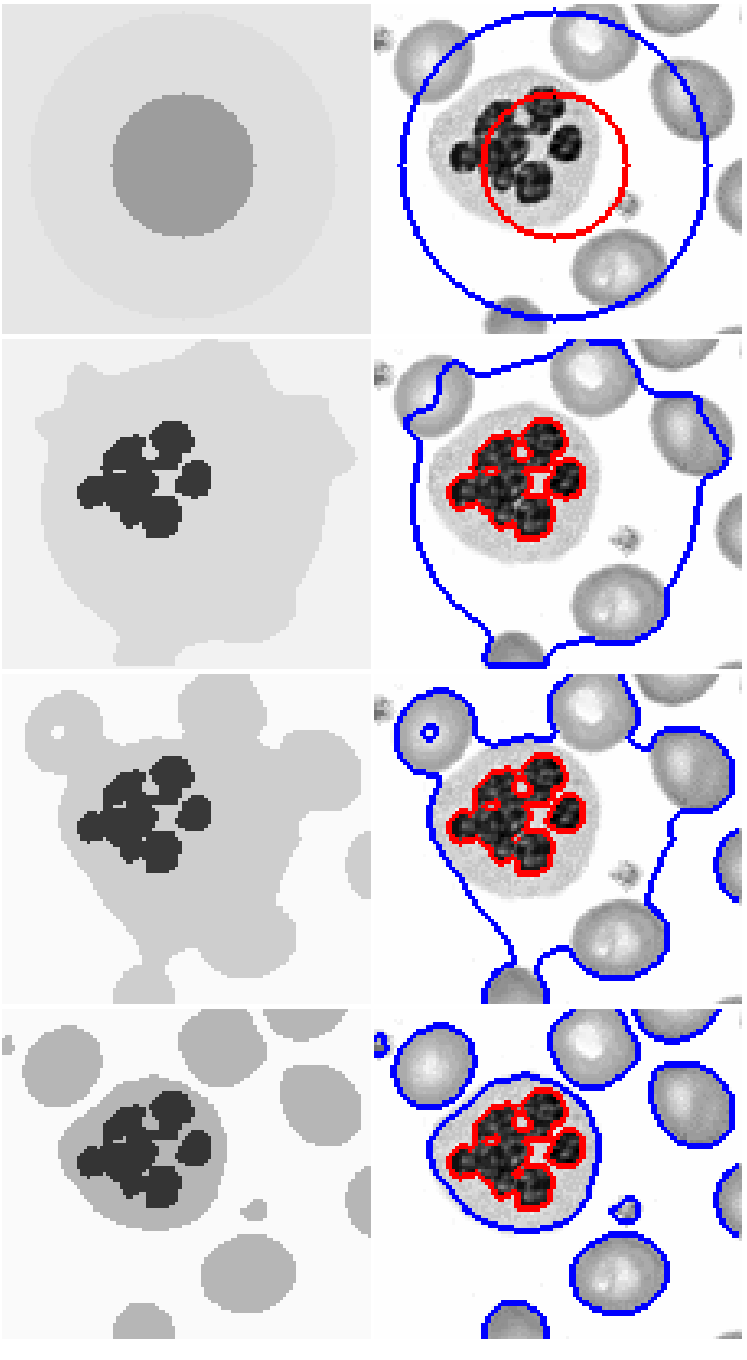

Fig. 4. Segmentation and denoising of a real noisy blood cells image using one level set function and two levels. Parameters: $l_1 = 0$, $l_2 = 25$, $\triangle t = 0.1$, $\mu = 0.043 \cdot 255^2$, 200 iterations, cpu time 2.493 sec.

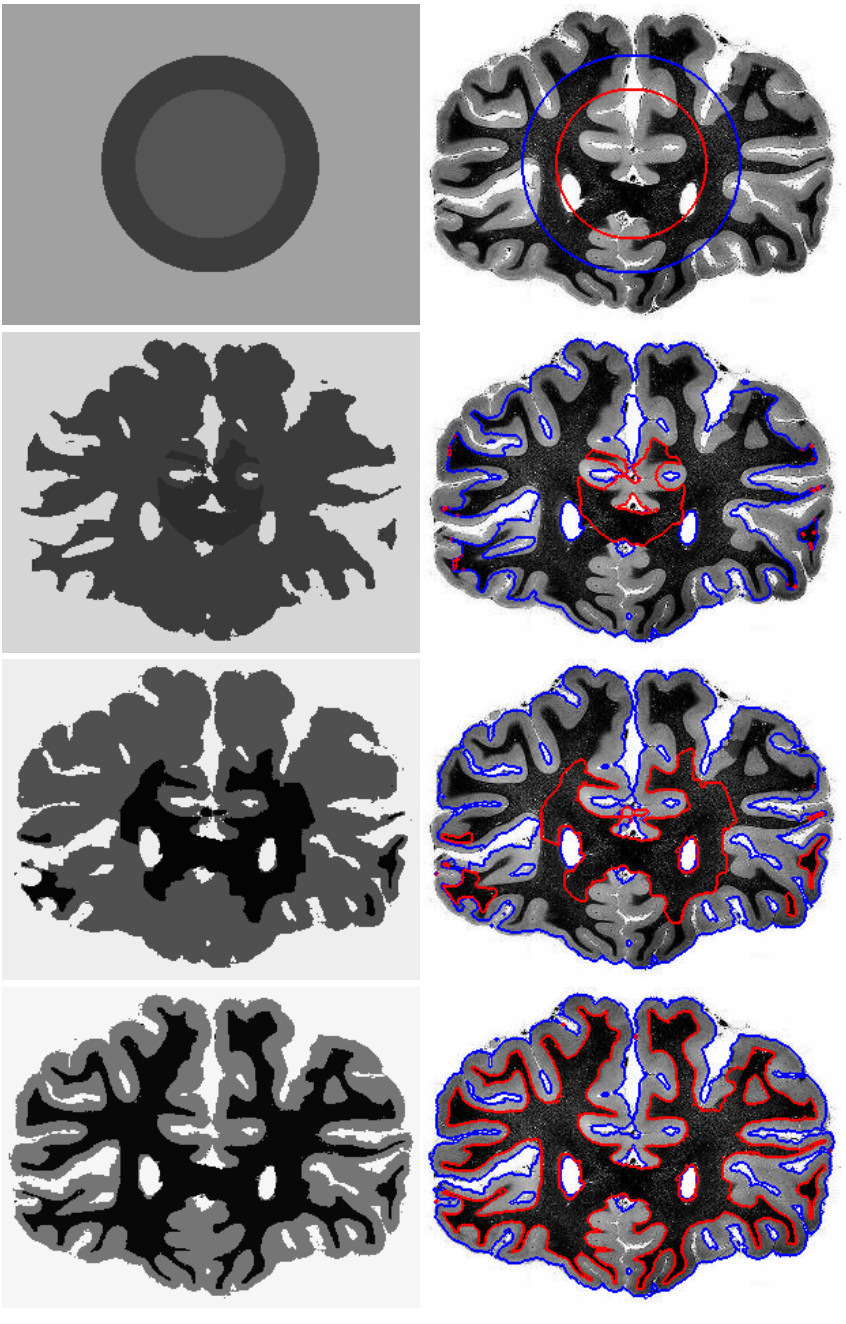

Fig. 5. Segmentation of a brain image using one level set function with two levels. Parameters: $l_1 = 0$, $l_2 = 25$, $\triangle t = 0.1$, $\mu = 0.1 \cdot 255^2$, 1500 iterations, cpu time 183.544 sec.

2.2 The Case of Two Functions

As in [11], [27], we can extend the multilayer model from the previous section to the case of more than one level set function. This may be needed for instance for images with triple junctions. Here, we will use only two level set functions, to represent up to nine distinct regions of different intensities, making up Ω. We will work with the functions ϕ_1 and ϕ_2, and with two levels $\{0,\ l\}$, with $l > 0$.

The nine regions defined by the two level set functions and two levels are:

$$R_{11} = \{x:\ \phi_1 < 0,\ \phi_2 < 0\}, R_{21} = \{x:\ 0 < \phi_1 < l,\ \phi_2 < 0\},$$
$$R_{31} = \{x:\ \phi_1 > l,\ \phi_2 < 0\},$$
$$R_{12} = \{x:\ \phi_1 < 0,\ 0 < \phi_2 < l\}, R_{22} = \{x:\ 0 < \phi_1 < l,\ 0 < \phi_2 < l\},$$
$$R_{32} = \{x:\ \phi_1 > l,\ 0 < \phi_2 < l\},$$
$$R_{13} = \{x:\ \phi_1 < 0,\ \phi_2 > l\}, R_{23} = \{x:\ 0 < \phi_1 < l,\ \phi_2 > l\},$$
$$R_{33} = \{x:\ \phi_1 > l,\ \phi_2 > l\}.$$

Following the previous section and [27], the associated energy for image segmentation is:

$$\begin{aligned}\inf_{\boldsymbol{c},\Phi} F(\boldsymbol{c},\Phi) = \int_\Omega \Big[&|f(x)-c_{11}|^2 H(-\phi_1(x))H(-\phi_2(x)) \\ &+|f(x)-c_{21}|^2 H(\phi_1(x))H(l-\phi_1(x))H(-\phi_2(x)) \\ &+|f(x)-c_{31}|^2 H(\phi_1(x)-l)H(-\phi_2(x)) \\ &+|f(x)-c_{12}|^2 H(-\phi_1(x))H(\phi_2(x))H(l-\phi_2(x)) \\ &+|f(x)-c_{22}|^2 H(\phi_1(x))H(l-\phi_1(x))H(\phi_2(x))H(l-\phi_2(x)) \\ &+|f(x)-c_{32}|^2 H(\phi_1(x)-l)H(\phi_2(x))H(l-\phi_2(x)) \\ &+|f(x)-c_{13}|^2 H(-\phi_1(x))H(\phi_2(x)-l) \\ &+|f(x)-c_{23}|^2 H(\phi_1(x))H(l-\phi_1(x))H(\phi_2(x)-l) \\ &+|f(x)-c_{33}|^2 H(\phi_1(x)-l)H(\phi_2(x)-l)\Big] dx \\ +\mu\Big[\int_\Omega |\nabla H(\phi_1)| + \int_\Omega |\nabla H(\phi_1-l)| &+ \int_\Omega |\nabla H(\phi_2)| + \int_\Omega |\nabla H(\phi_2-l)|\Big],\end{aligned}$$

where $\boldsymbol{c} = (c_{11}, c_{21}, c_{31}, c_{12}, c_{22}, c_{32}, c_{13}, c_{23}, c_{33})$ is the unknown vector of averages, and $\Phi = (\phi_1, \phi_2)$ is a vector-valued unknown function.

Embedding the minimization in a dynamical scheme, starting with $\phi_1(0,x) = \phi_{1,0}(x)$, $\phi_2(0,x) = \phi_{2,0}(x)$, we have that the unknown constants $c_{11}, c_{21}, ...$ are given by the averages of the data f on their corresponding regions $R_{11}, R_{21}, ...$, as follows:

$$c_{11}(t) = \frac{\int_\Omega f H(-\phi_1)H(-\phi_2)dx}{\int_\Omega H(-\phi_1)H(-\phi_2)dx},\ c_{21}(t) = \frac{\int_\Omega f H(\phi_1)H(l-\phi_1)H(-\phi_2)dx}{\int_\Omega H(\phi_1)H(l-\phi_1)H(-\phi_2)dx},$$
$$c_{31}(t) = \frac{\int_\Omega f H(\phi_1-l)H(-\phi_2)dx}{\int_\Omega H(\phi_1-l)H(-\phi_2)dx},\ c_{12}(t) = \frac{\int_\Omega f H(-\phi_1)H(\phi_2)H(l-\phi_2)dx}{\int_\Omega H(-\phi_1)H(\phi_2)H(l-\phi_2)dx},$$
$$c_{22}(t) = \frac{\int_\Omega f H(\phi_1)H(\phi_2)H(l-\phi_1)H(l-\phi_2)dx}{\int_\Omega H(\phi_1)H(\phi_2)H(l-\phi_1)H(l-\phi_2)dx},$$

$$c_{32}(t) = \frac{\int_\Omega f(x)H(\phi_1 - l)H(\phi_2)H(l-\phi_2)dx}{\int_\Omega H(\phi_1 - l)H(\phi_2)H(l-\phi_2)dx},$$
$$c_{13}(t) = \frac{\int_\Omega fH(-\phi_1)H(\phi_2 - l)dx}{\int_\Omega H(-\phi_1)H(\phi_2 - l)dx},$$
$$c_{23}(t) = \frac{\int_\Omega fH(\phi_1)H(l-\phi_1)H(\phi_2 - l)dx}{\int_\Omega H(\phi_1)H(l-\phi_1)H(\phi_2 - l)dx},$$
$$c_{33}(t) = \frac{\int_\Omega fH(\phi_1 - l)H(\phi_2 - l)dx}{\int_\Omega H(\phi_1 - l)H(\phi_2 - l)dx}.$$

The unknown functions ϕ_1 and ϕ_2 are solutions of the following equations:

$$\phi_1(0,x) = \phi_{1,0}(x), \quad \phi_2(0,x) = \phi_{2,0}(x),$$
$$\frac{\partial \phi_1}{\partial t} = \delta_\varepsilon(\phi_1)\Big[|f - c_{11}|^2 H(-\phi_2) - |f - c_{21}|^2 H(l - \phi_1)H(-\phi_2)$$
$$+|f - c_{12}|^2 H(\phi_2)H(l - \phi_2) - |f - c_{22}|^2 H(l - \phi_1)H(\phi_2)H(l - \phi_2)$$
$$+|f - c_{13}|^2 H(\phi_2 - l) - |f - c_{23}|^2 H(l - \phi_1)H(\phi_2 - l) + \mu \mathrm{div}\Big(\frac{\nabla \phi_1}{|\nabla \phi_1|}\Big)\Big]$$
$$+\delta_\varepsilon(\phi_1 - l)\Big[|f - c_{21}|^2 H(\phi_1)H(-\phi_2) - |f - c_{31}|^2 H(-\phi_2)$$
$$+|f - c_{22}|^2 H(\phi_1)H(\phi_2)H(l - \phi_2) - |f - c_{32}|^2 H(\phi_2)H(l - \phi_2)$$
$$+|f - c_{23}|^2 H(\phi_1)H(\phi_2 - l) - |f - c_{33}|^2 H(\phi_2 - l) + \mu \mathrm{div}\Big(\frac{\nabla \phi_1}{|\nabla \phi_1|}\Big)\Big],$$
$$\frac{\partial \phi_2}{\partial t} = \delta_\varepsilon(\phi_2)\Big[|f - c_{11}|^2 H(-\phi_1) - |f - c_{12}|^2 H(-\phi_1)H(l - \phi_2)$$
$$+|f - c_{21}|^2 H(\phi_1)H(l - \phi_1) - |f - c_{22}|^2 H(\phi_1)H(l - \phi_1)H(l - \phi_2)$$
$$+|f - c_{31}|^2 H(\phi_1 - l) - |f - c_{32}|^2 H(\phi_1 - l)H(l - \phi_2) + \mu \mathrm{div}\Big(\frac{\nabla \phi_2}{|\nabla \phi_2|}\Big)\Big]$$
$$+\delta_\varepsilon(\phi_2 - l)\Big[|f - c_{12}|^2 H(-\phi_1)H(\phi_2) - |f - c_{13}|^2 H(-\phi_1)$$
$$+|f - c_{22}|^2 H(\phi_1)H(l - \phi_1)H(\phi_2) - |f - c_{23}|^2 H(\phi_1)H(l - \phi_1)$$
$$+|f - c_{32}|^2 H(\phi_1 - l)H(\phi_2) - |f - c_{33}|^2 H(\phi_1 - l) + \mu \mathrm{div}\Big(\frac{\nabla \phi_2}{|\nabla \phi_2|}\Big)\Big].$$

We show in Fig. 6 an example of partition of the domain Ω, using two level lines corresponding to $l_1 = 0$, $l_2 = 10$, and two continuous functions ϕ_1, ϕ_2.

Note that, as in the multi-phase models from [27] and [28], when two distinct level set functions are used to represent the contours, as in this subsection, then it is possible that two level lines of the different functions ϕ_1 and ϕ_2 may partially overlap, and therefore by the above formulation the length of the common contour will be counted more than once and will have a different weight. This is different from the Mumford and Shah energy [20]. This is not a problem in practice, as seen in the numerical approximations. Moreover, this can also be simply avoided, as explained in [28].

We show next experimental results on images with triple junctions, where only two level set functions ϕ_1, ϕ_2 with two levels are used to represent up to nine disjoint regions, making up Ω.

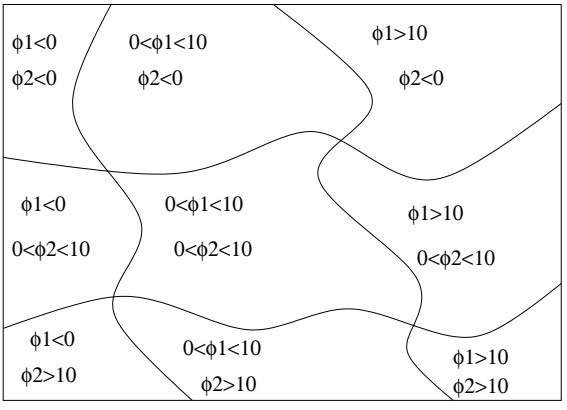

Fig. 6. The level lines $\{x \in \Omega : \ \phi_i(x) = 0\}$ and $\{x \in \Omega : \ \phi_i(x) = 10\}$, $i = 1, 2$, partition the domain Ω into 9 disjoint regions

We present in Fig. 7 a numerical result of segmentation and partition of a noisy synthetic image, composed of 5 regions of distinct intensities. All regions and corresponding intensities are correctly detected and represented. The model uses 9 phases in theory, but at steady state only 5 appear. The proposed model performs faster than the one in [27]; both multi-phase models give similar qualitative results. In Fig. 8 we have a numerical result for a noisy synthetic color image consisting of 9 regions of distinct intensities, in a vector-valued fashion, as in [8].

We note that in all the above numerical results, we do not use the reinitialization to the distance function of the level set functions ϕ, ϕ_i. Also, using the length regularization only of the level lines $\{\phi = l_i\}$, the function ϕ may become discontinuous away from these levels. This is true in practice, however, it does not appear to be an inconvenient. If, however, we would need to keep the function ϕ more regular, we can use different regularizations that act on all level lines of ϕ. We have tested and compared in practice several regularizations for ϕ, instead of the length of the levels l_i: these are $\int_\Omega |\nabla\phi| dx$ (total variation regularization, still decreases the perimeter of each level line independently, and produces a function ϕ that tends to be piecewise-constant, with jumps near the detected contours), $\int_\Omega |\nabla\phi|^2 dx$ (which will guarantee a smooth function ϕ, but may smooth corners also); $\||\nabla\phi|\|_{L^\infty(\Omega)}$, that leads to the infinity-Laplacian, or the second order derivative in the normal direction to the level lines of ϕ (this regularization formally keeps the function ϕ Lipschitz, in $W^{1,\infty}(\Omega)$, and the gradient magnitude is strictly positive near the contours, therefore preventing the surface to become too flat). All these regularizations give satisfactory and similar results. We conclude the paper by showing in Fig. 9 the iso-contours of the final function ϕ for the real image used in Fig. 4, obtained with length regularization, and with the sup-norm of the gradient regularization. We see that in the last case, the function ϕ is closer to a "distance" function, in the sense that distinct level lines stay at constant distance of each other, and do not become too close.

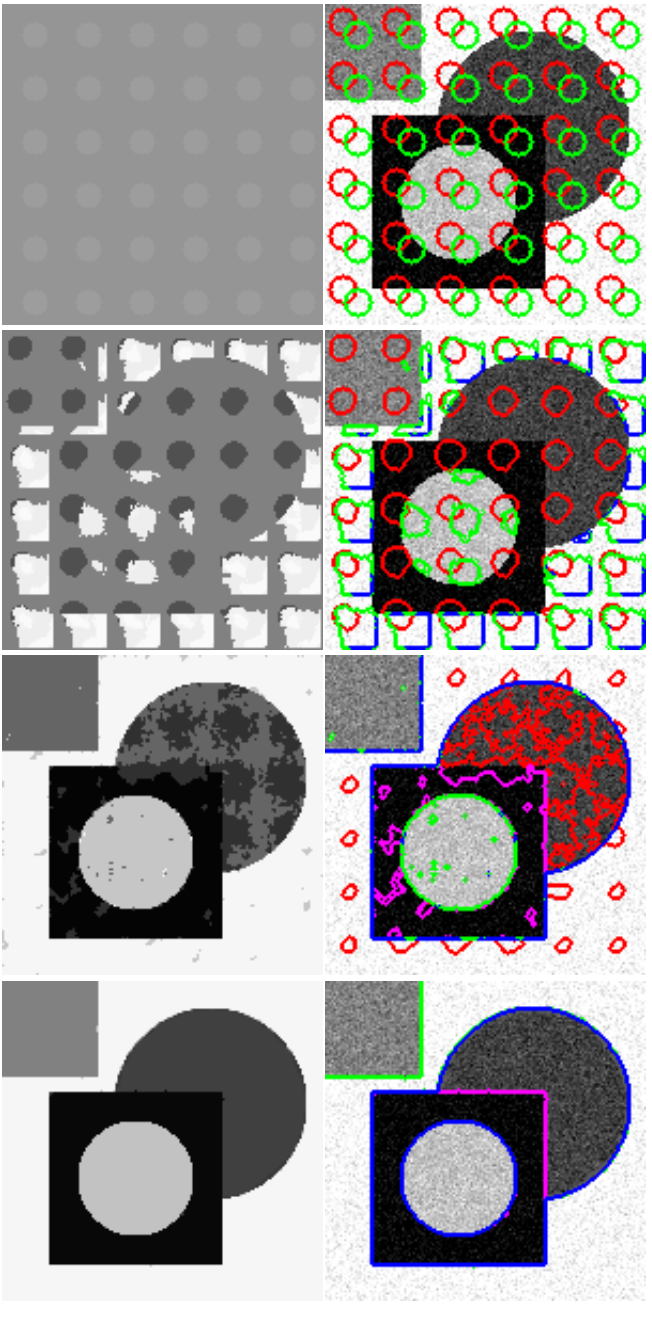

Fig. 7. Segmentation and denoising of a synthetic noisy image with triple junctions, using two functions ϕ_1, ϕ_2 and two levels. Parameters: $l_1 = 0$, $l_2 = 25$, $\triangle t = 0.4$, $\mu = 0.023 \cdot 255^2$, 200 iterations, cpu time 13.985 sec.

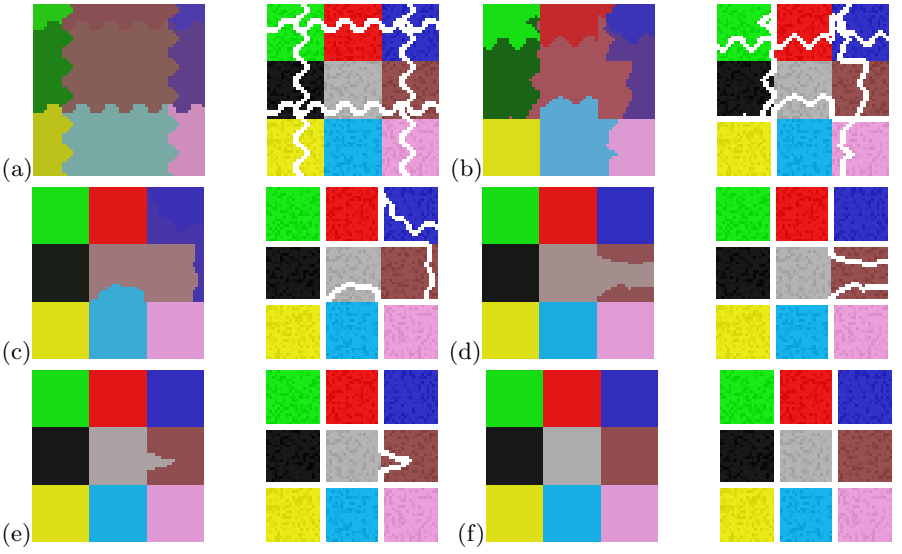

Fig. 8. Segmentation and denoising of a synthetic noisy color image with junctions, using two functions ϕ_1, ϕ_2 and two levels. Parameters: $l_1 = 0$, $l_2 = 25$, $\triangle t = 0.01$, $\mu = 0.335 \cdot 255^2$, 160 iterations, cpu time 10.975 sec. Note that the image contains nine different regions, all correctly detected and segmented in an efficient approach.

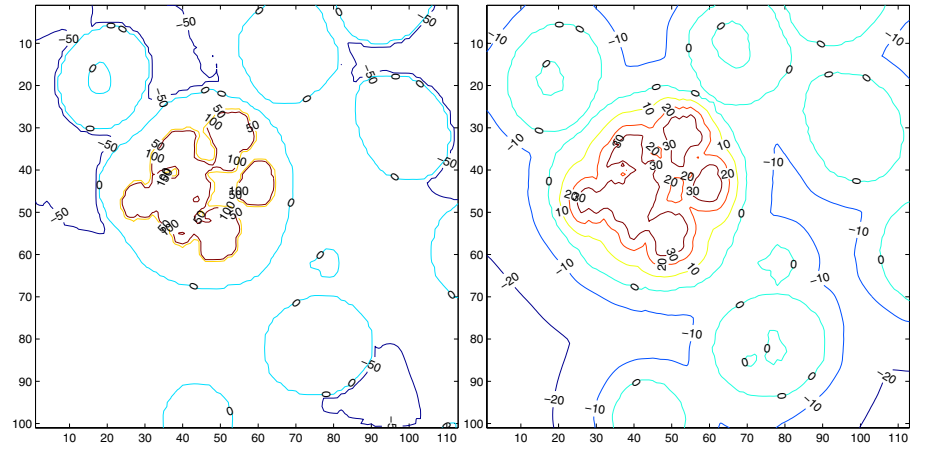

Fig. 9. Left: iso-contours of final ϕ using length regularization only, $\mu\delta_\varepsilon(\phi)\mathrm{div}\left(\frac{\nabla\phi}{|\nabla\phi|}\right) + \mu\delta_\varepsilon(\phi - l)\mathrm{div}\left(\frac{\nabla\phi}{|\nabla\phi|}\right)$. Right: iso-contours of final ϕ using the sup-norm of the gradient $\||\nabla\phi|\|_{L^\infty(\Omega)}$ as regularization, minimized using the infinity Laplacian $\mu\triangle_\infty\phi = \frac{\phi_{xx}(\phi_x)^2+2\phi_x\phi_y\phi_{xy}+\phi_{yy}(\phi_y)^2}{|\nabla\phi|^2}$, therefore ensuring that ϕ remains Lipschitz (see Aronsson [3], Caselles, Morel, Sbert [7], among others).

References

1. L. Ambrosio, V.M. Tortorelli, *Approximation of functionals depending on jumps by elliptic functionals via Γ-convergence*, Comm. Pure Appl. Math., 43, 999-1036, 1990.
2. L. Ambrosio, V.M. Tortorelli, *On the Approximation of Free Discontinuity Problems*, Bollettino U.M.I. (7) 6-B, 105-123, 1992.
3. G. Aronsson, *Minimization problems for functionals* $\sup_x F(x, f(x), f'(x))$, Arkiv for mathematik 6(1): 33-&, 1965.
4. R.E. Caflisch, M.F. Gyure, B. Merriman, S.J. Osher, C. Ratsch, D.D. Vvedensky, J.J. Zinck, *Island dynamics and the level set method for epitaxial growth*, Applied Mathematics Letters 12(4): 13-22, 1999.
5. V. Caselles, F. Catté, T. Coll, F. Dibos, *A geometric model for active contours in image-processing*, Numerische Mathematik, 66(1): 1-31, 1993.
6. V. Caselles, R. Kimmel, G. Sapiro, *Geodesic active contours*, IJCV 22(1): 61-79, 1997.
7. V. Caselles, J.M. Morel, C. Sbert, *An axiomatic approach to image interpolation*, IEEE Transactions on IP 7(3): 376-386, 1998.
8. T.F. Chan, B.Y. Sandberg, L.A. Vese, *Active contours without edges for vector-valued images*, JVCIR, 11(2): 130-141, 2000.
9. T. F. Chan, L. Vese, *An active contour model without edges*, LNCS 1682, 141-151, 1999.
10. T.F. Chan, L.A. Vese, *Active contours without edges*, IEEE Transactions on IP 10(2): 266 -277, 2001.
11. T.F. Chan, L.A. Vese, *Level Set Algorithm for Minimizing the Mumford-Shah Functional in Image Processing*, IEEE Workshop on VLSM, 161-168, 2001.
12. L.D. Cohen, *Avoiding local minima for deformable curves in image analysis*, in *Curves and Surfaces with Applications in CAGD*, A. Le Méhauté, C. Rabut, and L.L. Schumaker (eds.), 77-84, 1997.
13. L. Cohen, E. Bardinet, and N. Ayache, *Surface reconstruction using active contour models*, Proc. SPIE 93 Conference on Geometric Methods in Computer Vision, San Diego, CA, July 1993.
14. M.F. Gyure, C. Ratsch, B. Merriman, R.E. Caflisch, S. Osher, J.J. Zinck, D.D. Vvedensky, *Level-set methods for the simulation of epitaxial phenomena*, Physical Review E 58(6): R6927-R6930 Part A, 1998.
15. S. Kichenassamy, A. Kumar, P. Olver, A. Tannenbaum, A. Yezzi Jr., *Conformal curvature flows: from phase transitions to active vision*, Arch. Rational Mech. Anal. 134(3): 275–301, 1996.
16. G. Koepfler, C. Lopez, J.-M. Morel, *A multiscale algorithm for image segmentation by variational method*, SIAM J. Num. Analysis, 31(1): 282-299, 1994.
17. J. Lie, M. Lysaker, X.-C. Tai, *Piecewise Constant Level Set Methods and Image Segmentation*, LNCS 3459: 573-584, 2005.
18. R. Malladi, J.A. Sethian, B.C. Vemuri, *Shape modeling with front propagation - a level set approach*, IEEE Tr. PAMI, 17(2): 158-175, 1995.
19. J.M. Morel, S. Solimini, *Density estimates for the boundaries of optimal segmentations*, CRASS I-Mathématique 312(6): 429-432, 1991.
20. D. Mumford, J. Shah, *Optimal approximation by piecewise smooth functions and associated variational problems*, Comm. Pure Appl. Math. 42:577-685, 1989.
21. N. Paragios, R. Deriche, *Unifying boundary and region-based information for geodesic active tracking*, Proc. CVPR 1999, Vol. 2: 23-25, 1999.

22. N. Paragios, R. Deriche, *Geodesic active regions: A new framework to deal with frame partition problems in computer vision*, JVCIR 13(1-2): 249-268, 2002.
23. N. Paragios, R. Deriche, *Geodesic active regions and level set methods for supervised texture segmentation*, IJCV 46(3): 223-247, 2002.
24. C. Samson, L. Blanc-Féraud, G. Aubert, J. Zérubia, *A level set model for image classification*, LNCS 1682, 306-317, 1999.
25. C. Samson, L. Blanc-Féraud, G. Aubert, J. Zérubia, *A level set model for image classification*, IJCV 40(3): 187-197, 2000.
26. A. Tsai, A. Yezzi, A.S. Willsky, *Curve evolution implementation of the Mumford-Shah functional for image segmentation, denoising, interpolation, and magnification*, IEEE Transactions on IP, 10(8):1169 - 1186, 2001.
27. L.A. Vese and T.F. Chan, *A Multiphase Level Set Framework for Image Segmentation Using the Mumford and Shah Model*, IJCV 50(3): 271-293, 2002.
28. L. Vese, *Multiphase Object Detection and Image Segmentation* in "Geometric Level Set Methods in Imaging, Vision and Graphics", S. Osher and N. Paragios (eds), Springer Verlag, 175-194, 2003.
29. H.-K. Zhao, T. Chan, B. Merriman, and S. Osher, *Variational level set approach to multiphase motion*, JCP 127(1): 179-195, 1996.
30. S.C. Zhu and A. Yuille, *Region competition: Unifying snakes, region growing, and Bayes/MDL for multiband image segmentation*, IEEE Transactions on PAMI, 18(9): 884-900, 1996.